CHAPTER 2

GRAIN OPTICAL PROPERTIES

Martha Hanner
Jet Propulsion Laboratory

with contributions from D. R. Huffman, N. Divine,
S. Green, P.L. Lamy, D. Lien, and K. Sellgren

1.0 INTRODUCTION

The optical properties of small grains provide the link between the infrared observations presented in Chapter 1 and the dust composition described in Chapter 3. In this session, the optical properties were discussed from the viewpoint of modeling the emission from the dust coma and the scattering, at $\lambda \leq 2.5\mu$m, in order to draw inferences about the dust-size distribution and composition.

The optical properties are applied to the analysis of the infrared data in several ways, and these different uses should be kept in mind when judging the validity of the methods for applying optical constants to real grains.

1) Computing grain temperature:

The equilibrium temperature of a grain in the solar radiation field is computed by equating the total energy absorbed to the total energy radiated

$$\pi s^2 \left(\frac{R_\odot}{R}\right)^2 \int_\odot^\infty Q_{abs}(s,\lambda) S(\lambda) d\lambda = 4\pi s^2 \int_\odot^\infty \pi B(\lambda, T) Q_{abs}(s,\lambda) d\lambda$$

where $S(\lambda)$ is the solar flux, $B(\lambda,T)$ the Planck function at grain temperature T, R is the heliocentric distance, and Q_{abs} (s,λ) the wavelength-dependent absorption efficiency factor for grain radius s. For this purpose the Q_{abs} are required from the ultraviolet through the infrared for any grain size; however, the accuracy required is not stringent. In fact, for absorbing grains, the resulting grain temperatures depend primarily on grain size, not on the detailed wavelength dependence of the complex refractive index.

From the computed temperatures (as a function of grain size) and the grain size distribution, the infrared flux can be calculated and compared with the observed flux to derive the dust production rate.

2) Predicting the infrared spectral energy distribution:

Here, the interest lies in identifying the physical nature of the grains – their composition, size and other attributes such as degree of crystallinity. Spectral features are of particular interest. For this purpose, one needs not only good optical constants, but also a means of applying them to real grains, with all their bumps and blemishes.

3) Analyzing the scattered light and polarization:

At wavelengths $\lambda \leq 2.5\mu$m, scattered light dominates the radiation from the coma. Here, the angular scattering functions $i_1(\phi)$, $i_2(\phi)$ are required, and these are strongly affected by grain shape and surface irregularity.

Although simpler than the case of circumstellar dust in the sense that the geometry is known and the optical depth is low, the comet analysis is complicated by the range of grain sizes, which tends to obscure the band structure diagnostic of composition. Moreover, the large range of grain sizes means that the Rayleigh approximation is never valid, in contrast to interstellar grains in the far infrared.

Our discussion at this workshop focused on the availability of appropriate optical constants and the adequacy of theories to apply them to real grains. Some first attempts to fit the infrared data with models based on optical constants were reported. The grain-size distribution, as measured by the spacecraft, and its compatibility with the infrared data were also discussed. The analysis of comet dust was contrasted with the case of interstellar dust in reflection nebulae.

2.0 OPTICAL CONSTANTS

To interpret the infrared observations, optical constants are required not only in the infrared, but also in the visible and near-uv in order to compute the equilibrium temperature of small grains in the solar radiation field. By optical constants we mean the complex dielectric functions, or equivalently the complex refractive indices, as a function of wavelength.

Huffman stressed the amount of effort required to determine optical constants correctly in the laboratory. Optical measurements, such as reflectance and/or transmittance must be performed as a function of wavelength on a polished bulk sample and an appropriate theory (such as Fresnel's equations) is then used to compute the optical constants as a function of wavelength. The optical constants cannot adequately be measured directly on small particles, in part because of the problems of clustering, as discussed in Section 2.5.

Among the materials relevant for cometary dust are silicates, various forms of carbon, magnetite, and organic materials. All of these have at least some measured optical constants. While ices are also of interest, they were not addressed at this workshop.

2.1 Silicates

As described in Chapter 1, spectra of Halley's dust coma exhibit a prominent 8- to 12.5 μm emission feature with peaks indicative of crystalline olivine and pyroxene. This is in contrast to earlier comet spectra and almost all relevant spectra of interstellar and circumstellar sources, which show a broad, structureless feature, leading to the conclusion that the grains must be amorphous. However, the Halley spectra are consistent with the composition and infrared spectra of interplanetary dust particles (IDPs), which clearly show signatures of crystalline olivine and pyroxene minerals (Sandford and Walker 1985; Sandford, Chapter 3, this report).

It was emphasized at the Workshop that one should not think only of two end states, but rather a continuous range of structural order. Indications of crystallinity will be evident in the 10μm stretching mode vibrations for a greater degree of disorder than in the 20μm bending mode vibration. This is a possible explanation for the lack of a distinct peak in the 20μm Halley spectrum. An example of the changing 10μm spectrum during annealing is given by Day (1974). Thus, optical constants for silicates with differing degrees of structural order are desirable.

Refractive indices of crystalline silicates are tabulated by Pollack *et al.* (1973) for natural samples of obsidian, basalt, and andesite from 0.2 to 0.50μm. Steyer (Ph.D. thesis 1974) determined the optical constants of several silicates from 0.2 to 50μm, including

the three major polarization directions of crystalline olivine, $[Mg,Fe]_2\ SiO_4$. Mooney and Knacke (1985) have measured refractive indices from 2.5 to 50μm for natural samples of the hydrated silicates chlorite and serpentine.

Kratschmer and Huffman (1979) derived the optical constants for a disordered olivine by irradiating polished crystals of olivine with high-energy neon ions until the crystal structure in the optically active surface layer was destroyed. In this way, the smooth surface was preserved for reflectance measurements. Classical dispersion theory was used to derive the optical constants from 8 to 25 microns. The extinction of amorphous silicate smokes from 7 to 300 microns has been measured by Day (1976, 1979, 1981), but optical constants approximated from Day's extinction measurements and those extrapolated from Kratschmer and Huffman's work are badly discrepant. A direct determination of optical constants for disordered olivine at long wavelengths is desirable.

2.2 Carbon

Graphitic carbon (as opposed to diamond-like carbon) can occur in a complete range of structural order from totally amorphous on one end to single-crystal graphite on the other. Graphite was originally suggested as a component of interstellar grains because it shows a feature near the position of the 2200Å interstellar feature. However, recent laboratory work has shown that less structured forms of carbon can produce a similar feature (e.g., Borghesi *et al.* 1985; Sakata *et al.* 1983). Furthermore, graphite is rarely seen in interplanetary dust particles, although carbonaceous material is common.

Single-crystal graphite is anisoptropic. Reliable optical constants exist for the easy-to-measure E$\perp$c direction (Taft and Philipp 1965; Philipp 1977). The E$\|$c is much more difficult because of the difficulty of preparing a polished sample for the reflectance measurements, and existing measurements are quite discrepant. But modeling using only the E$\perp$c optical constants overestimates the absorption in the ultraviolet, for example, compared to an ensemble of randomly oriented graphite grains.

In choosing a material representative of partially disordered carbon, Edoh (1983) selected for study the homogeneous bulk material called glassy or vitreous carbon. It is available commercially and is capable of being highly polished to permit proper optical measurements to be made. The ultraviolet region had already been well measured by Williams and Arakawa (1972).

Edoh prepared polished samples of glassy carbon and performed specular reflectance measurements, overlapping and agreeing well with the previous measurements. The usual Kramers-Kronig analysis of the combined reflectance data set produced the optical constants contained in Table 2-1 and plotted in Figure 2.1. These may prove useful to modelers needing optical constants for a type of carbon having a partial degree of order intermediate between single-crystal graphite and completely disordered carbon. Details of these measurements are found in the 1983 Ph.D. thesis of Edoh, which can be cited as the source reference until the measurements appear in a published journal article.

2.3 Magnetite

Magnetite is a candidate cometary material which is present in meteorites. It has the interesting property that infrared optical constants change with temperature. Steyer (1974) determined the optical constants from 2 to 100 microns for the same samples which Huffman and Stapp (1973) measured in the ultraviolet (see Huffman 1977, Fig. 33); these refer to room temperature.

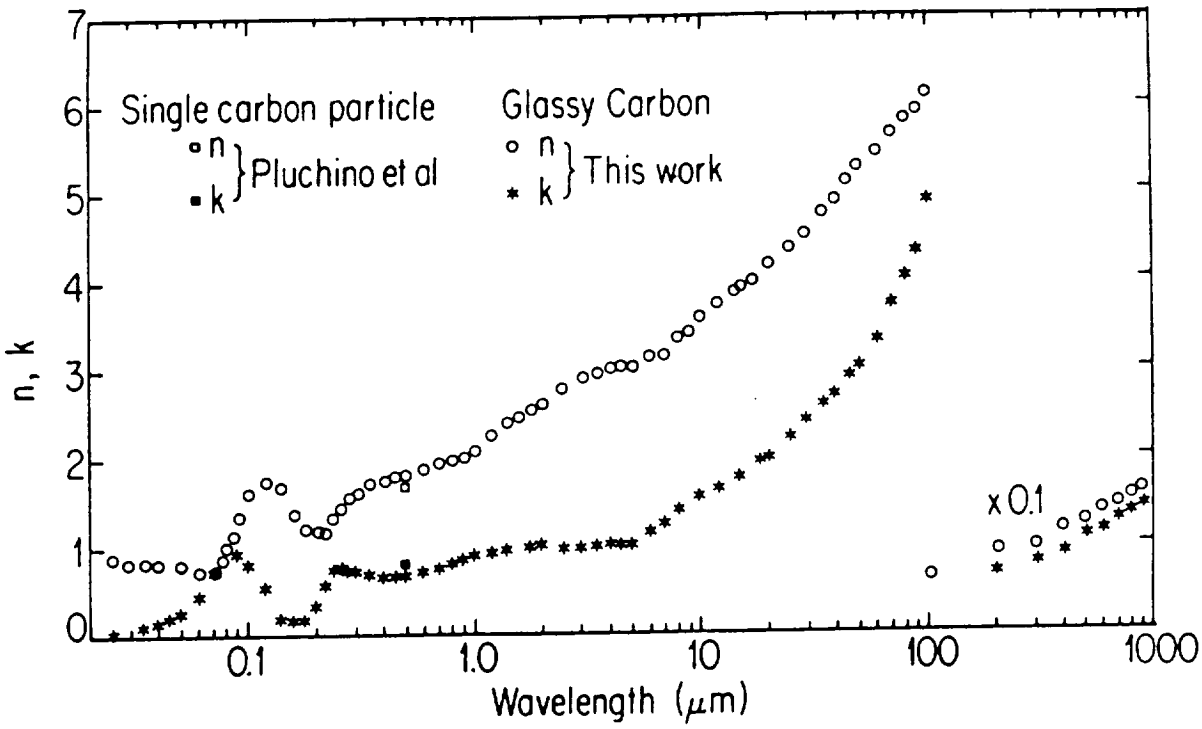

Figure 2.1 - Optical constants n and k of glassy carbon as computed by the Kramers-Kronig method (Edoh 1983).

Table 2-1

OPTICAL PROPERTIES OF CARBON FROM THE FAR INFRARED TO THE FAR ULTRAVIOLET

$\lambda(\mu m)$	n	k	$\lambda(\mu m)$	n	k
.04	.84	.108	11.	3.63	1.60
.05	.74	.177	12.	3.70	1.63
.06	.69	.380	13.	3.75	1.69
.07	.76	.66	14.	3.84	1.74
.08	.93	.90	15.	3.88	1.78
.09	1.26	.95			
.10	1.53	.84	16.	3.96	1.83
.12	1.74	.56	17.	3.99	1.89
.14	1.70	.202	18.	4.1	1.95
.16	1.39	.151	19.	4.14	1.95
.18	1.24	.180	20.	4.18	1.98
.20	1.22	.321			
			21.	4.22	2.03
.22	1.19	.57	23.	4.31	2.08
.24	1.34	.74	25.	4.36	2.19
.26	1.46	.74	27.	4.47	2.27
.28	1.54	.73	29.	4.53	2.37
.30	1.60	.72			
.30	1.60	.72	31.	4.61	2.42
.35	1.70	.69	33.	4.67	2.52
.40	1.75	.67	35.	4.77	2.60
.45	1.79	.67	37.	4.82	2.67
.50	1.82	.68	39.	4.91	2.72
.60	1.88	.71	41.	4.96	2.81
.70	1.94	.77	43.	5.04	2.85
.80	2.00	.80	45.	5.11	2.92
			50.	5.25	3.00
.90	3.45	.85			
.92	2.04	.86	55.	5.32	3.18
.94	2.04	.87	60.	5.44	3.31
.96	2.06	.89	65.	5.49	3.50
.98	2.06	.90	70.	5.67	3.70
1.0	2.11	.90	75.	5.71	3.80
1.2	2.24	.95	80.	5.85	4.00
1.4	2.38	.97	85.	5.90	4.15
1.6	2.46	.99	90.	5.99	4.30
1.8	2.55	1.00	95.	5.94	4.48
2.0	2.63	1.02	105.	6.7	4.7
2.5	2.80	1.00	205.	8.6	6.5
3.0	2.86	.99	305.	10.2	8.0
3.5	2.95	1.01	405.	11.6	9.5
4.0	3.03	1.04	505.	12.6	10.5
5.0	3.04	1.03	605.	13.4	11.6
			705.	14.1	12.5
6.0	3.15	1.15	805.	15.0	13.4
7.0	3.16	1.25	905.	16.5	14.1
8.0	3.35	1.42			
9.0	3.42	1.47			
10.	3.55	1.54			

2.4 Organic Materials

Optical constants from 0.02 to 1000μm have been determined by Khare *et al.* (1984) for a dark organic solid produced by electrical discharge in a gas mixture of 0.9 N_2 and 0.1 CH_4 ("Titan tholin"). The imaginary part of the refractive index, k is ~0.04 at 0.5μm and decreases to 4 x 10^{-4} at 1.5 microns, causing a reddish color and classifying this as a "slightly absorbing" material. The real part of the refractive index at visible wavelengths is ~1.68, similar to silicates; thus, this tholin resembles the "dirty silicate" in the visible.

Recently, Khare *et al.* (1987) have measured optical constants in the visible and near-infrared (0.35-2.5μm) for several other tholins produced by electrical discharge in pure methane gas and in H_2 gas with varying methane abundance. The synthesized products have similar optical properties, with n in the range 1.56 - 1.67 and $10^{-4} < k < 10^{-2}$ at $\lambda > 0.5\mu$m, similar also to the Titan tholin. Refractive indices for various carbonaceous materials at $\lambda = 0.5\mu$m are summarized in this reference.

Optical measurements are in progress for another organic residue produced by irradiating gas and ice mixtures similar to cometary ices in initial composition (Khare *et al.* 1987b). For a product synthesized from a gas mix of equal parts methane and water, they find n = 1.48 - 1.58 and k = 2 x 10^{-3} to 4 x 10^{-2} at 0.5μm.

While there are many infrared spectra of organic residues showing features near 3.4μm, optical constants are needed for this region, to allow modeling as a function of grain-size distribution and temperature.

In general, one would expect the optical constants (especially the absorptivity) to depend on the radiation dose, which determines the C/H ratio of the material. Coloration and progressive darkening with increasing irradiation are noted by almost all experimenters.

2.5 Relating Extinction Measurements to Optical Constants: The Problem of Clustering

One would think that optical constants could be derived from measured extinction, scattering, absorption directly on small particles. However, in cases where extinction has been computed, based on the optical constants measured on bulk samples, and compared with extinction measured in the laboratory for small particles, the results are disconcertingly discrepant. Much of this problem is apparently due to particle-clustering (Bohren & Huffman 1983, Huffman 1987 and abstract, this report). Huffman proposed that the shape distribution for randomly oriented ellipsoids in the Rayleigh limit is an appropriate way to treat the problem of clustering (see Section 3.3).

2.6 Optical Constants in the Far Infrared

Carbon: The optical constants of Edoh may be satisfactory to represent disordered carbon at wavelengths $\leq 100\mu$m. The effects of clustering are expected to become increasingly important in carbon at longer wavelengths ($> 100\mu$m) because of the increasing values of both real and imaginary parts of the dielectric functions.

Silicates: Pollack *et al.* present optical constants of crystalline silicates out to 50μm, while Steyer's measurements extend to 300 microns. No reliable optical constants exist for amorphous silicate beyond ~25μm. Several general trends of optical constants for insulators such as silicate are expected at long wavelength (Huffman 1977; Mitra and Nudelman 1970):

(1) In single crystals, absorption should decrease steeply with a magnitude that is quite temperature-dependent (lower absorption at low temperatures).

(2) In disordered (amorphous) insulators absorption is generally much higher than for single crystals, is less steep in wavelength dependence, and much less dependent on temperature.

(3) Impurities will lead to higher absorption.

(4) The effects of clustering are expected to become constant in insulators at long wavelength.

Organic Materials: A slightly absorbing material, such as the "Titan tholin," will follow the general behavior of an insulator. For the Titan tholin, the real part of the refractive index increases slightly and the imaginary part decreases from 0.2 to 0.002 from 100 to 1000 microns.

2.7 Recommendations for Further Measurements

Measurements of optical constants for disordered silicates from 25 to 100μm are needed, not only to define the wavelength dependence, but also to indicate any features in the 24 to 40μm region.

Because both silicates and carbon can occur with a range from complete disorder to fully crystalline, it is important to document the degree of disorder in the measured samples.

Measurements are desirable that would help to define the structure in both the 10- and 20-micron silicate bands for olivine and pyroxene as a function of the degree of disorder.

Optical constants, as opposed to transmission and reflectance spectra, are needed for appropriate organic materials in the 3μm region.

One needs to be aware of the discrepancies that can be caused by particle clustering, in particular when attempting to deduce optical constants from extinction measurements.

3.0 APPLICATION OF OPTICAL CONSTANTS

Once the optical constants as a function of wavelength have been specified, an appropriate theory must be applied to predict the observable radiation from the ensemble of cometary particles. While we have many reasons to believe that cometary dust particles are not perfect spheres (one has only to look at the IDPs), most interpretations rely on the theory of spheres to solve for the interaction of light with the particles. Generalization of this theory to non-spherical particles is a formidable task which is being approached slowly from the theoretical and experimental viewpoints.

It does not appear, at the present time, that the problem can be treated in a unified way; as a consequence, we have to distinguish different situations for which we have some understanding of the interaction. We discuss here examples of theoretical approaches which were presented at the Workshop; other approaches exist in the literature.

3.1 Smooth Spheres

The interaction of light with a smooth, homogeneous spherical particle can be computed from Mie theory. Descriptions are given by Kerker (1969), van de Hulst (1957), Bohren and Huffman (1983). For our purposes, we need to understand the extent to which Mie theory is useful in predicting the behavior of non-spherical particles, specifically in predicting grain temperatures, infrared emissivity (continuum, features) and scattering.

The problem also has been solved analytically for other smooth, geometric shapes, such as spheroids and infinite cylinders, by expressing the boundary conditions in the

appropriate coordinates.

3.2 Rough Non-Spherical Particles

Particles Smaller than the Wavelength

For particles smaller than the wavelength, but larger than the Rayleigh limit, the best approach appears to rely on the representation of the particle by a network of interacting dipoles, as pioneered by Purcell and Pennypacker (1973). This has recently been improved by Chiapetta, Perrin, and Torresani (1987) and their model is able to reproduce the phase functions $i_1(\theta)$ and $i_2(\theta)$ of a perfect sphere as given by Mie theory. It remains to be seen how the model will behave when more complex shapes are introduced. It is important to realize that, in this case, the roughness is much less than the wavelength.

Large Rough Particles (s> λ)

When the roughness scale is comparable to or larger than the wavelength, several effects, such as diffraction, multiple reflection, and shadowing enter the interaction. Perrin and Lamy (1986) have obtained a solution for this problem in the framework of the potential theory, introducing a statistical description of the roughness. In its most elaborate form, a vectorial description is obtained enabling one to calculate not only the efficiency factors but also the polarization. This theory is able to produce remarkably well the experimental data of Weiss-Wrana (1983) for non-absorbing as well as absorbing material (see Fig. 2.4).

It must be kept in mind that this solution holds for large rough particles, with a conservative lower limit of particle radius $s/\lambda \geq 6$.

The effect of the roughness in terms of optical properties is illustrated in Figure 2.2, where the efficiency factors for a 50μm astronomical-silicate grain (Draine 1985) are plotted as a function of the mean roughness for various wavelengths (0.25, 0.5, 3, 10μm). Of importance is the substantial rise in the efficiency factors with respect to the "canonical" Mie values (roughness = 0), the differing behavior as a function of wavelength resulting from the complex index of refraction. Note that the Q_{abs} is less affected than Q_{scat} and Q_{ext}, a trend noted also in an analytic treatment by Wiscombe and Mugnai (1980).

A direct consequence is that rough grains of this "dirty" silicate absorb more energy in the visible than spheres, therefore reaching a somewhat higher equilibrium temperature. A preliminary calculation (Lamy, in preparation) is shown in Figure 2.3, where the temperature of "dirty" silicate grains at 1 AU is plotted versus their radius; for s= 100μm, the increase reaches 30 K, or about 10%.

Other consequences concern the phase function, which generally exhibits a broader diffraction lobe, and the polarization. Figure 2.4 compares the predictions from this theory with scattering by a 14μm slightly absorbing particle from the Allende meteorite measured by Weiss-Wrana (1983). One sees that the theory correctly predicts the width of the forward-scattering peak and the rise toward 180 deg, as well as the magnitude of polarization. The observed polarization of the dust coma of Halley can be matched approximately by a mixture of rough silicate and graphite particles, as illustrated in Figure 2.5 (Lamy *et al.* 1987). It is important to emphasize that, in this theory, the negative polarization branch is caused by the surface roughness of the absorbing grains, which does not exist for absorbing spheres; the surface roughness reduces the large (both positive and negative) polarization of the (dielectric) silicate grains.

3.3 Treatment of Shape Effects

Shape effects can be important, even in very small particles, in regions where surface modes are important (Bohren & Huffman Chapter 12). Two cases of direct relevance to

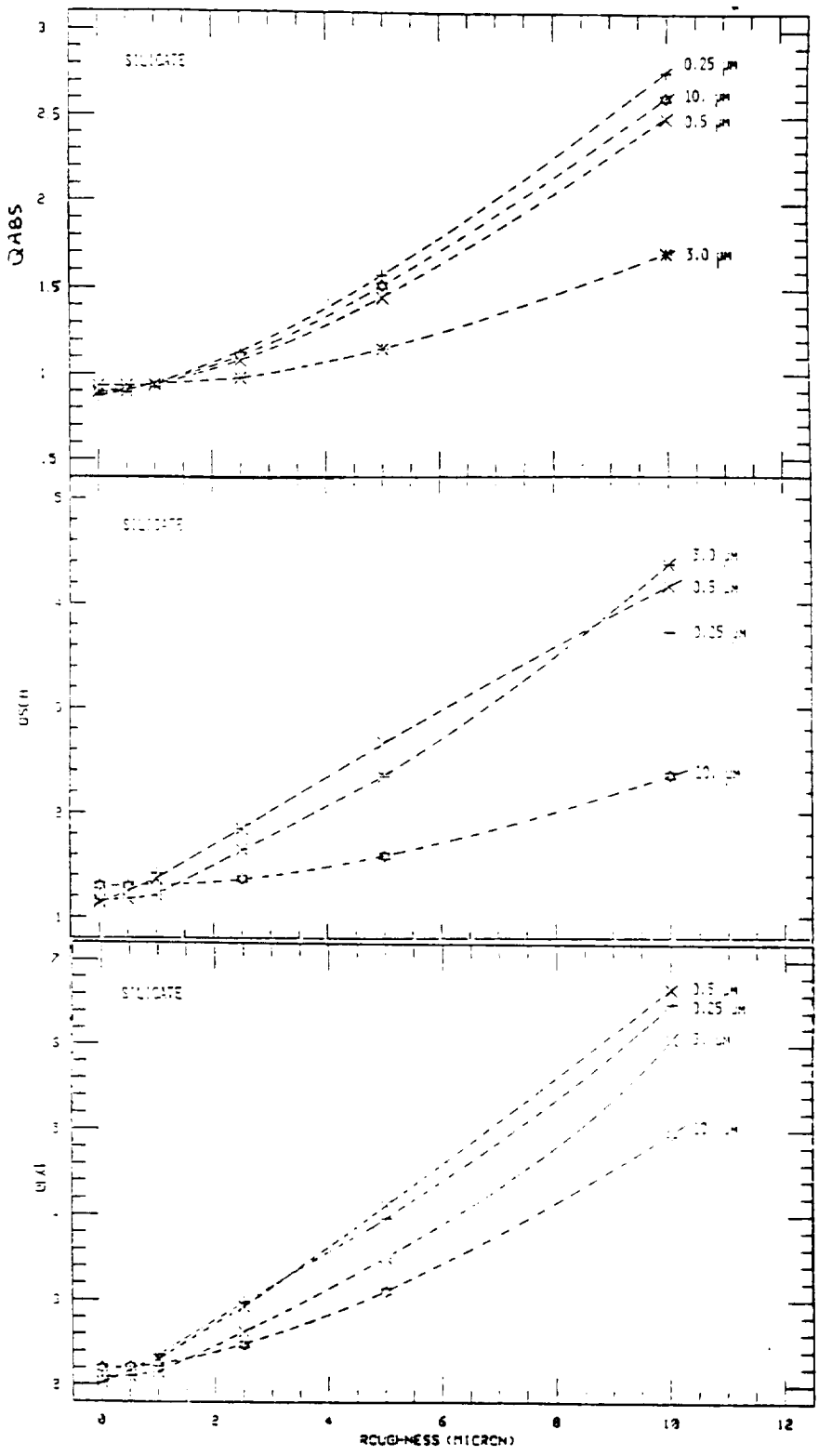

Figure 2.2 - Efficiency factors as a function of roughness for a 50μm silicate particle at various wavelengths (Lamy, abstract this report).

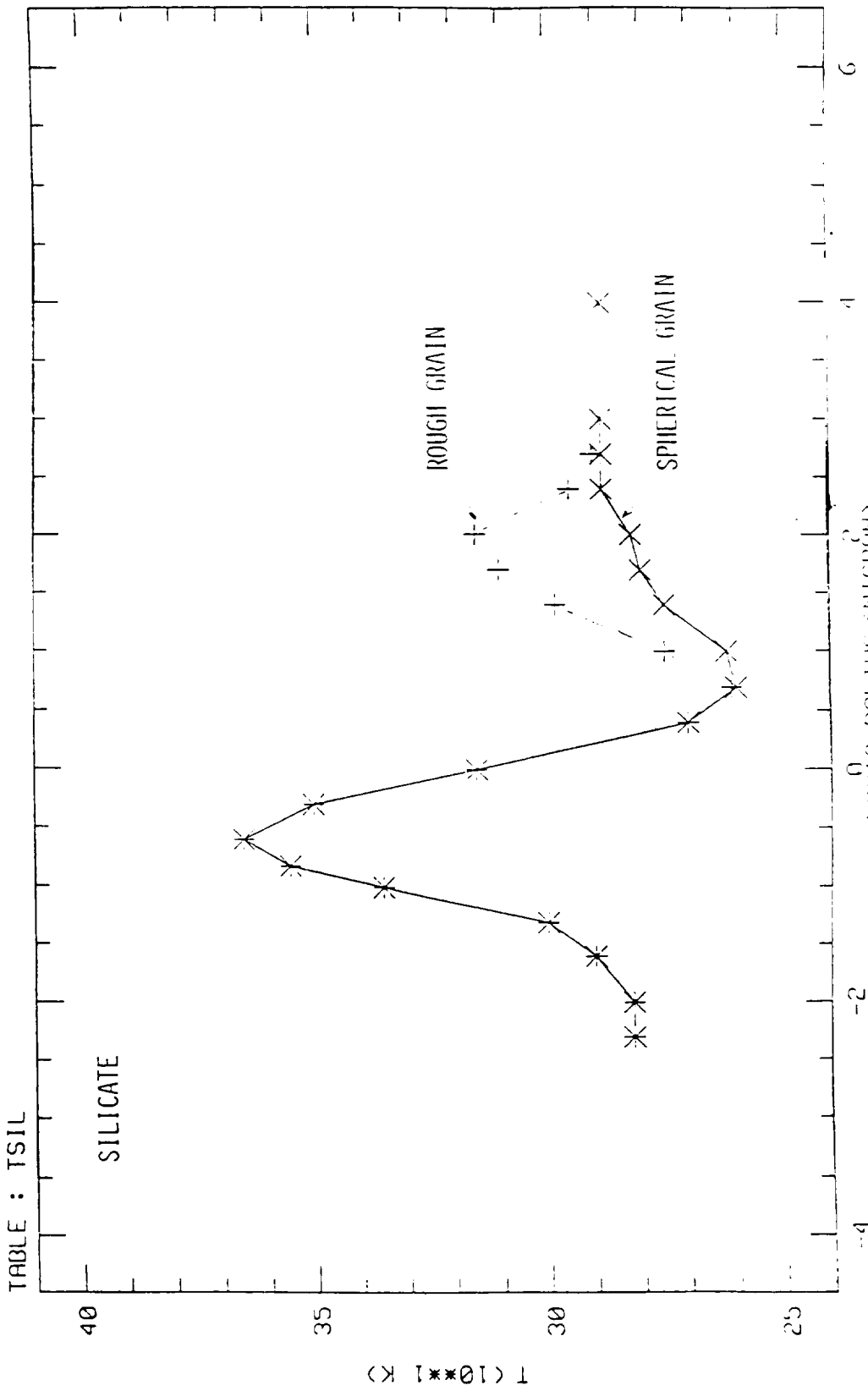

Figure 2.3 - Temperature of "astronomical" silicate grains at 1 AU, as a function of particle size for the spherical and rough cases.

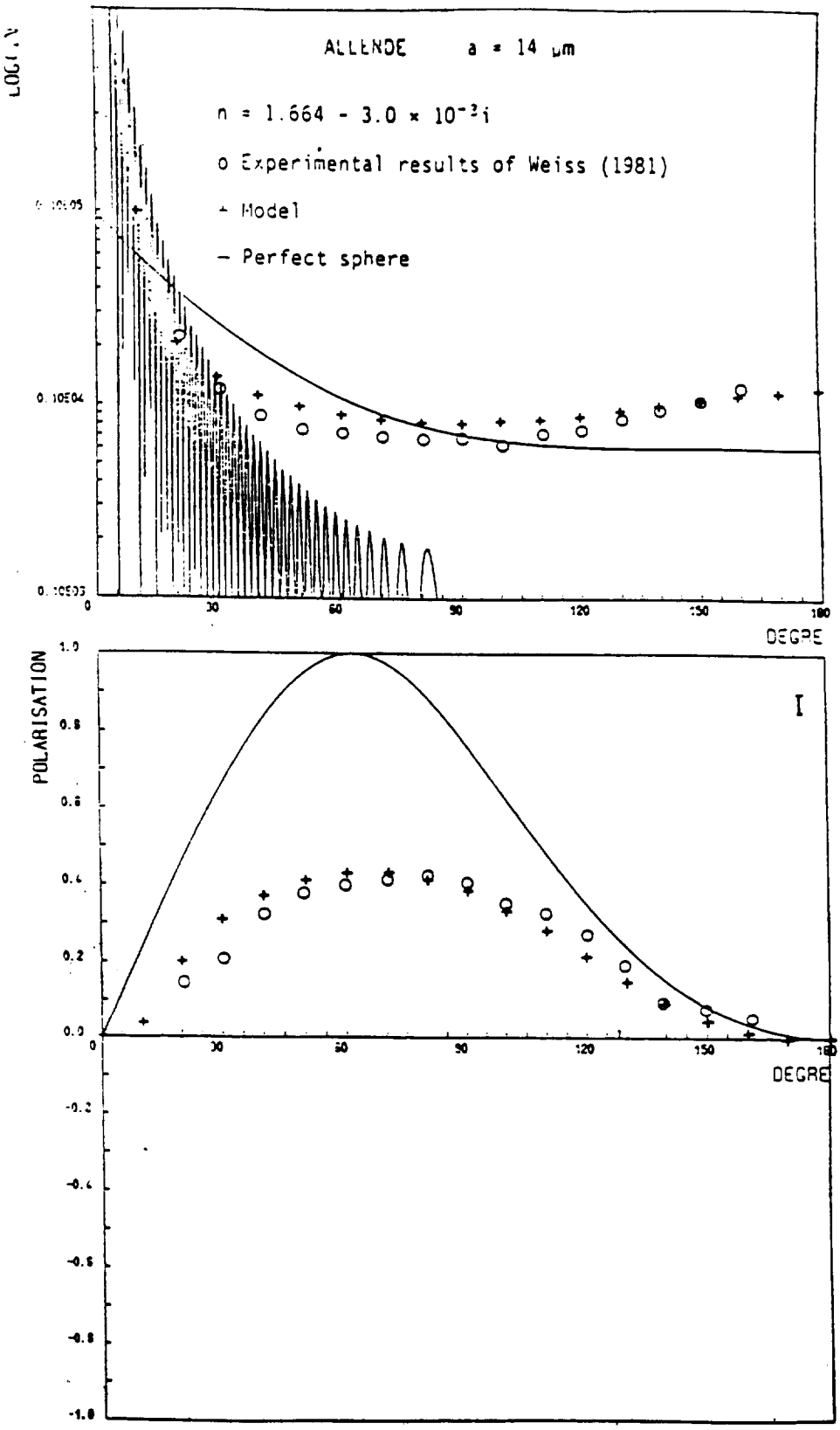

Figure 2.4 - Comparison of theory for rough particles (+) with optical measurements on a particle from the Allende meteorite (Perrin and Lamy 1983).

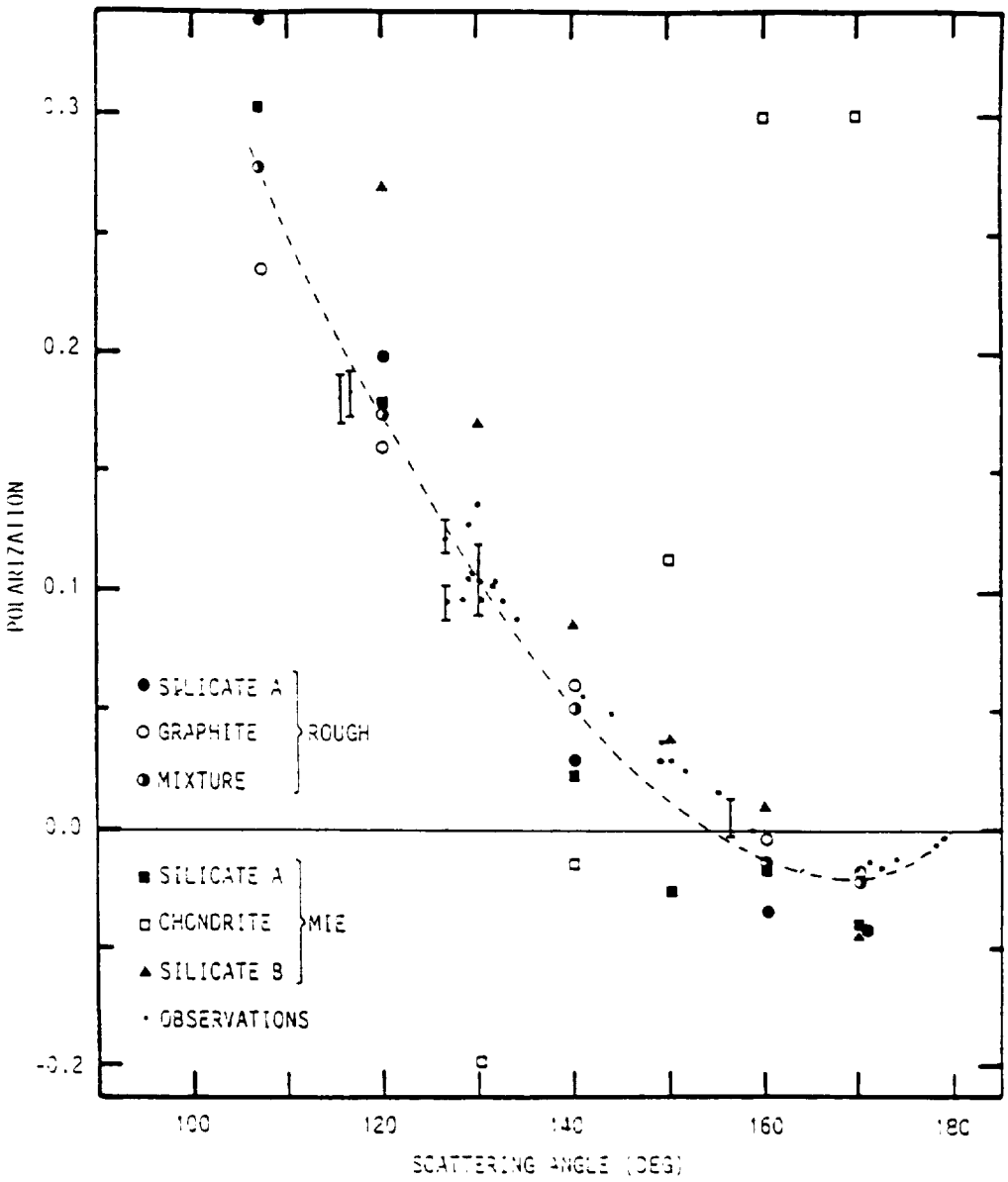

Figure 2.5 - Polarization of Comet Halley (Lamy *et al.* 1987). The small dots are the observational data from Mukai *et al.* (1986), Dollfus *et al.* (1986). A mixture of rough silicate and graphite grains gives the best fit to the data.

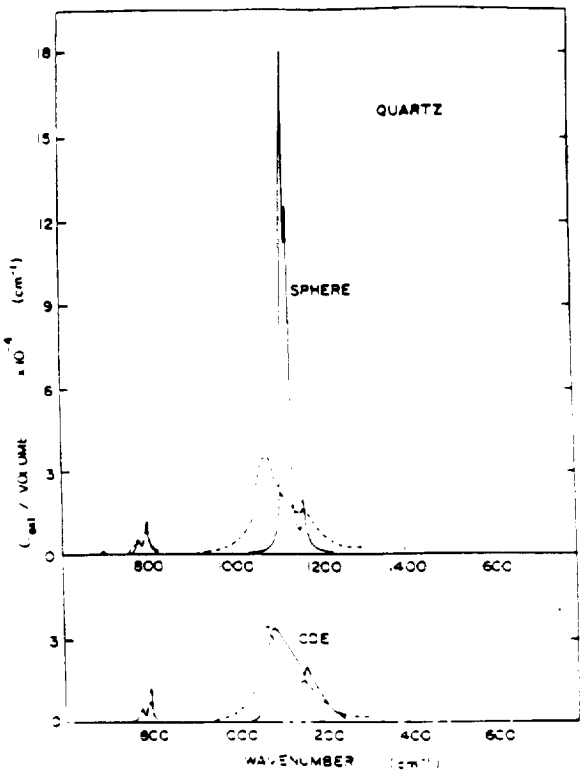

Figure 2.6 - Measured extinction of crystalline quartz particles compared with calculations for spheres and CDE (Bohren and Huffman 1983).

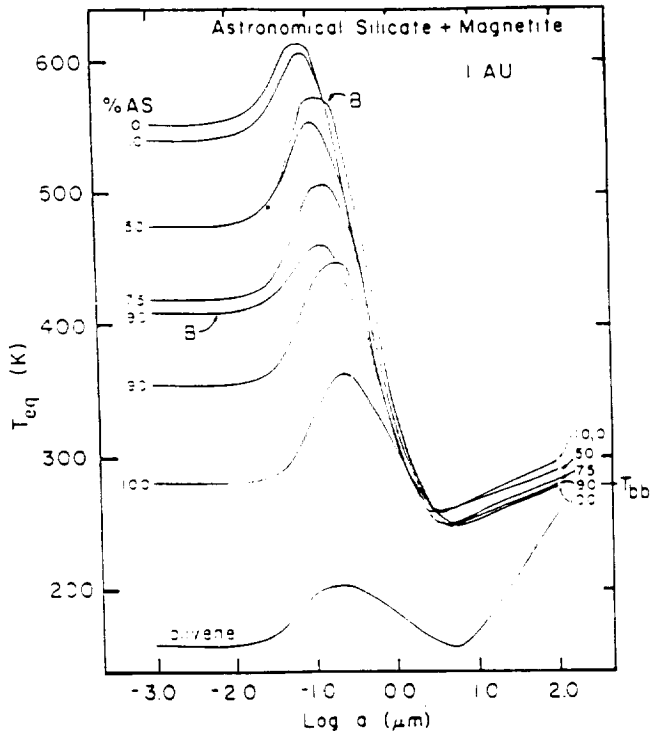

Figure 2.7 - Equilibrium grain temperatures at 1 AU computed for blends of "astronomical" silicate and magnetite, based on Maxwell-Garnett theory and Bruggeman theory (B) (Lien 1987).

the infrared data were discussed in which shape effects can cause significant deviation from the predictions of Mie theory. One case is the 10μm silicate resonance, the other the behavior of the far-infrared emissivity.

Huffman described a relativly simple approach which seems to permit reasonable calculations to be made for clustered particles. Known as the CDE model, this method treats the particles as a continuous distribution of ellipsoidal shape parameters, in the Rayleigh limit. The expression for the volume-normalized absorption cross section, averaged over all ellipsoid orientations and all possible shape parameters, reduces to:

$$\frac{\ll \text{Cabs} \gg}{\text{v}} = \text{k Im} \frac{(2\epsilon \log\epsilon)}{\epsilon - 1}$$

where ϵ is the complex dielectric constant. An example for the 9μm resonance in crystalline quartz is displayed in Figure 2.6 (Bohren & Huffman 1983; Huffman, abstract this report). One sees that the CDE theory comes far closer to predicting the correct height, width, and central wavelength of the measured extinction feature. However, the CDE theory has been less successful when applied to measurements of an olivine smoke; thus, its usefulness for relating the cometary 10μm spectrum-to-optical properties of silicate minerals is not clear. (See Section 3.5).

The Far-Infrared

Most crystalline materials exhibit a $1/\lambda^{-2}$ falloff in extinction at long λ, while various interstellar measurements suggest a less steep decrease, perhaps $1/\lambda$. Laboratory measurements of carbon by Koike *et al.* (1980) also seem to show a falloff more like $1/\lambda$. Huffman (1987) explains this discrepancy as caused by particle clustering and shows (see abstract this report) that the CDE treatment, using the optical constants of glassy carbon measured by Edoh (1983), duplicates the slope of the laboratory-smoke measurements.

Thus, particle shape appears to be a significant factor in determining the long-wavelength emissivity. Further comparisons with laboratory measurements for well-defined particle shape distributions (fractals?) are clearly important. A more detailed discussion, and further examples, can be found in Bohren & Huffman, Chapter 12, and Huffman (1987).

3.4 Non-Homogeneous Particles

Two conceptual models for computing the average dielectric functions of nonhomogeneous grains were discussed. In the Bruggeman theory the composite grain is considered to be a mixture of small grains randomly packed together, while in the Maxwell-Garnett theory the composite grain consists of small inclusions (x<<1) embedded in a matrix material. The theories can be generalized to more than two components. Their limitations have been discussed by Bohren (1986).

Lien reported on calculations performed using these two theories for composite grains consisting of "astronomical" silicate (Draine 1985) and magnetite. Temperatures computed for spherical grains at 1 AU are plotted in Figure 2.7 as a function of the percent silicate included in a magnetite matrix (Lien 1987). (The "astronomical" silicate already has a higher absorption at visible wavelengths than pure silicate, leading to a warmer temperature than pure olivine.)

It is evident that even the addition of 10% of an absorbing material such as magnetite raises the temperature significantly, and a 50-50 mix is almost indistinguishable from pure magnetite, except at the smallest grain sizes. (Note that for larger grains, s > 10μ, the temperature dip is reversed in rough particles – see Fig. 2.3).

Strictly, these effective medium theories assume that the component particle sizes are much smaller than the wavelength. These theories suffer from the same problems already discussed when near a resonance in the optical constants of one component.

3.5 10-Micron Silicate Feature

The 10-micron region in the Halley spectra is extremely difficult to treat analytically. There are two serious problems, either one of which alone could be fatal to a quantitative model. First, Mie theory does not adequately predict the structure and strength of the 10μm feature in irregularly-shaped crystalline silicate particles. Second, it is likely that the comet grains have varying degrees of crystallinity, which are not adequately represented by the optical constants for the end members alone. Complicating the picture further, it appears that more than one kind of silicate is present and contributing to the observed feature. While the optical constants for olivine have been measured rather well, the same cannot be said for other silicates, such as enstatite, a pyroxene mineral known to be present in IDPs. Moreover, the silicate grains in the comet seem likely to be embedded in carbonaceous material.

No easy answers emerged from this workshop. Analogy with the spectra of IDPs, as discussed by Sandford (this report), may be the best approach available to identify the kinds of silicates present. A detailed quantitative analysis of the Mg:Fe:Si ratios, relative abundances and size distribution of the silicates in comet dust, will be possible by direct sampling from the Comet Rendezvous mission.

3.6 Core-Mantle Particles

Although not discussed specifically at this workshop, calculations for layered spheres, while still suffering from the limitations of Mie theory, may be of some use in predicting the general effects of absorbing material overlying silicate particles, for example.

3.7 Laboratory Studies

Laboratory measurements of the interaction of irregular particles are an important means of testing the validity of analytical treatments. Their drawback is that it is difficult to generalize from the specific laboratory experiment to particles in astrophysical contexts, as the above discussion of clustering effects illustrated.

Considerable work has been done on measurement of the scattering and polarization of irregular particles of relevance to cometary grains. Much of this has been accomplished by scaling the particle size and wavelength to microwave frequencies (e.g., Schuerman 1980a; Zerull *et al.* 1980). Larger particles have been suspended and studied with lasers. These studies support the results of Lamy and Perrin regarding the shape of the phase function and the negative polarization branch. Obtaining the efficiency factors, Q_{scat} and Q_{ext} from these scattering measurements is not always possible, however, because the laboratory setup often does not allow measurement of the forward scattering lobe where much of the energy is concentrated.

Many extinction measurements have been made at infrared wavelengths. These are useful to the extent that the measured particle ensemble resembles that in the comet (size distribution, shape distribution, composition, degree of crystallinity). One should also be aware that extinction is not equal to absorption in cases where scattering may be important, since $Q_{ext} = Q_{abs} + Q_{scat}$.

Interplanetary dust particles are an important resource for understanding optical/ir grain properties. Their composition can be directly related to their infrared spectra and

their measured optical properties can be compared with predictions based on optical constants.

3.8 Other Sources

Considerable theoretical and experimental research is taking place for other applications of particle optical properties which may be relevant for interpreting the optical and infrared observations of comet dust (see for example Schuerman (1980)).

Each year, for about ten years now, the U.S. Army Chemical Research Development and Engineering Center (CRDEC) has sponsored a conference called the "Scientific Conference on Obscuration and Aerosol Research." These have brought together an impressive group of workers in the field of small-particle optical research. Both theory and experiments relating to spherical and nonspherical particles have been presented. Numerous measurements of optical constants have been reported, including natural silicates and carbons. It may be of value for astronomical studies of particles to become familiar with the results of this annual conference, as reported in the publications listed in Table 2-2.

3.9 Summary

These points emerged from the discussion:

- For a compact, homogeneous particle with surface irregularity smaller than the wavelength, the absorption efficiency, Q_{abs}, is not badly approximated by Mie theory, provided the wavelength is not near a strong feature. As the roughness increases, the Q_{abs} will increase.
- The temperature of a large rough particle under solar illumination will be somewhat higher than that of an equivalent smooth sphere, because of the higher Q_{abs}.
- The CDE model for a random distribution of ellipsoids shows promise for treating the far-infrared emissivity; further laboratory comparisons are desirable.
- Effective medium theory for deriving optical constants of heterogeneous material can be useful for investigating the approximate optical and thermal properties of composite grains (e.g., silicates + absorbing material; crystalline + amorphous silicates).
- An adequate analytical treatment for predicting the shape of the 10- and 20-micron silicate features does not exist.
- Particle roughness is particularly important for polarization, and the polarization versus phase angle for an irregular particle is not well represented by Mie theory.
- Polarization can be treated by a theory for rough particles; surface roughness introduces a negative polarization branch for absorbing particles and reduces the polarization in silicates.
- Surface roughness can explain the observed scattering phase function, including the enhanced backscattering.
- The Q_{abs} and scattering for a fractal grain model should be explored.
- Analytical methods can be tested by attempting to reproduce measured infrared spectra of IDPs.
- Astronomers should not ignore the considerable research on light interaction with irregular particles being conducted in other fields, for example the research funded by the Army.

TABLE 2-2

Previous Proceedings

of the CSL/CRDC* Scientific Conference

on Obscuration and Aerosol Research

Chemical Research, Development and Engineering Center

Aberdeen Proving Ground, Maryland 21010-5423

Year of Conference	Report Number
1979	ARCSL - CR - 81023
1980	ARCSL - SP - 82021
1981	ARSCL - SP - 82022
1982	ARCSL - SP - 83011
1983	CRDC - SP - 84009
1984	CRCD - SP - 85007
1985	CRDEC - SP - 86019

*The U.S. Army Chemical Research, Development and Engineering Center (CRDEC) was known as the Chemical Research and Development Center (CRDC) prior to March 1986 and as the Chemical Systems Laboratory (CSL) prior to July 1983.

4.0 DUST-SIZE DISTRIBUTION

4.1 *In-Situ*-Mass Distribution

The Vega and Giotto spacecraft carried detectors to record the impact rate and mass distribution of dust particles. Since the spacecraft velocity of $\sim$ 70 km/s was far larger than the outflow velocity of the dust, the sensors sampled the spatial density of the dust, a quantity needed for modeling the infrared emission. While a generally consistent picture emerges, all of the sensors detected changes in the mass distribution along the trajectory, with steeper slope (more small particles) generally associated with higher impact rates (dust jets). The abundant small particles ($\sim$ 0.01μm) discovered by the flyby missions contribute negligibly to the infrared thermal continuum or scattered light.

Divine described the cumulative mass distributions from the spacecraft data and the analytical expressions he has applied to them. He has fit the various integral mass distributions with a function which approximates two power-law segments, using the parameters and formulae specified in Table 2-3. These are discussed further in his abstract, this volume, and Divine and Newburn (1987). Some additional useful quantities are defined in Table 2-4.

The Giotto Dust Impact Detector (DIDSY) used momentum sensors attached to the spacecraft dust shield to detect particle masses $\geq 4\text{x}10^{-10}$ g. The sensor response to impacts on the shield was calibrated pre-flight by several techniques. A momentum enhancement factor of 11 was used to account for the ejected target material, based on prior experimental and analytical studies (McDonnell *et al.* 1984). To form a complete mass curve, the DIDSY fluences were joined to those recorded by the Particle Impact Analyzer at masses 10^{-12} to 10^{-16} g (McDonnell *et al.* 1987). This composite distribution and Divine's curve are displayed in Figure 2.8. The cumulative mass exponent is equal to 0.94.

The fluences recorded by the SP-2 instruments on Vega 1 and 2 are shown in Figure 2.9, along with Divine's analytical curve. SP-2 utilized impact plasma sensors for the mass range $10^{-16} - 10^{-11}$ g and momentum sensors for 3×10^{-13} to 10^{-6} g (Mazets *et al.* 1986). In-flight calibration was performed by comparing the two data sets in the overlapping mass range and assuming a momentum enhancement factor of 5. For the impact velocity of 78 km/s, the momentum enhancement is probably closer to 11 (McDonnell *et al.* 1984); thus the curves in Figure 2.9 should probably be shifted toward smaller mass by a factor 2 (factor of 1.3 in radius). It can be seen that Vega 1, which encountered stronger jet activity than Vega 2, measured a steeper mass distribution. The SP-1 experiment, an impact plasma sensor with different geometry, gave similar slope and impact rate for m $< 10^{-10}$ g (Vaisberg *et al.* 1986).

On the other hand, the DUCMA experiment, which used a PVDF detector, recorded steeper slopes in the mass range 10^{-13} to 10^{-11} g (Simpson *et al.* 1986). This discrepancy remains unresolved.

4.2 Large Particles

The DIDSY sensors effectively used the entire dust shield as a sounding board, thus enabling the detection of large particles, including those that penetrated the front shield. The mass distribution for these large particles shows a very flat slope (McDonnell *et al.* 1987). Crifo (1987) has pointed out that this flat slope is inconsistent with the observed thermal emission spectrum. Green reported on the efforts to understand this enhancement of large particles and reconcile the DIDSY data with the Giotto radio science experiment and earth-based infrared observations (Perry, Green, McDonnell abstract this report).

Giotto DIDSY and radio-science data represent observations of dust originating from a narrow track along the nucleus, the smallest observed grains being emitted $\sim$ one hour pre-

TABLE 2-3

DUST SIZE DISTRIBUTION

QUANTITY	SYMBOL / FORMULA	UNITS
Particle Mass (variable)	m	(kg)
Transition Mass (parameter)	m_t	(kg)
Dummy Variable	$x = (m/m_t)^{1/\gamma}$	
Exponent for Large Mass	α	
Exponent Ratio, Small/Large Masses	β	
Transition Sharpness Parameter	γ	
Distribution Coefficient	F_t	(m^{-2})
Integral Number Fluence (mass > m, or size > a)	$F = F_t \left[\frac{(1+x)^{\beta-1}}{x\beta}\right]^{\alpha\gamma}$	(m^{-2})
Differential Number Fluence (per mass interval)	$f_m = \left(\frac{\alpha F_t}{m_t}\right)\frac{(\beta+x)(1+x)^{(\beta-1)\alpha\gamma-1}}{x^{(\alpha\beta+1)\gamma}}$	($m^{-2}kg^{-1}$)
Radius	$a = \left(\frac{3m}{4\pi\rho}\right)^{1/3} = a_t x^{\gamma/3}$	(μm)
Differential Number Fluence (per radius interval)	$f_a = \left(\frac{3\alpha F_t}{a_t}\right)\frac{(\beta+x)(1+x)^{(\beta-1)\alpha\gamma-1}}{x^{(\alpha\beta+1/3)\gamma}}$	($m^{-2}\mu m^{-1}$)

RELATIONS: $f_m = -\frac{dF}{dm} = -\frac{dx}{dm}\frac{df}{dx}$, $f_a = \frac{dm}{da} f_m$, and $F = \int_m^\infty dm\, f_m = \int_a^\infty da\, f_a$

TABLE 2-4

SIZE DISTRIBUTION: LIMITING DEPENDENCES $\left[x = (m/m_t)^{1/\gamma} = (a/a_t)^{3/\gamma}\right]$

For $\beta = 1$ (any x) or Large $x \gg 1$ (any β) ($m \gg m_t$ and $a \gg a_t$)	For $\beta \neq 0$ and Small $x \ll 1$ (any $\beta > 0$) ($m \ll m_t$ and $a \ll a_t$)
$F = F_t x^{-\alpha\gamma} = F_t\left(\frac{m_t}{m}\right)^{\alpha} = F_t\left(\frac{a_t}{a}\right)^{3\alpha}$	$F = F_t x^{-\alpha\beta\gamma} = F_t\left(\frac{m_t}{m}\right)^{\alpha\beta} = F_t\left(\frac{a_t}{a}\right)^{3\alpha\beta}$
$f_m = \frac{\alpha F_t}{m_t} x^{-(\alpha+1)\gamma} = \frac{\alpha F_t}{m_t}\left(\frac{m_t}{m}\right)^{\alpha+1}$	$f_m = \frac{\alpha\beta F_t}{m_t} x^{-(\alpha\beta+1)\gamma} = \frac{\alpha\beta F_t}{m_t}\left(\frac{m_t}{m}\right)^{\alpha\beta+1}$
$f_a = \frac{3\alpha F_t}{a_t} x^{-(\alpha+1/3)\gamma} = \frac{3\alpha F_t}{a_t}\left(\frac{a_t}{a}\right)^{3\alpha+1}$	$f_a = \frac{3\alpha\beta F_t}{a_t} x^{-(\alpha\beta+1/3)\gamma} = \frac{3\alpha\beta F_t}{a_t}\left(\frac{a_t}{a}\right)^{3\alpha\beta+1}$

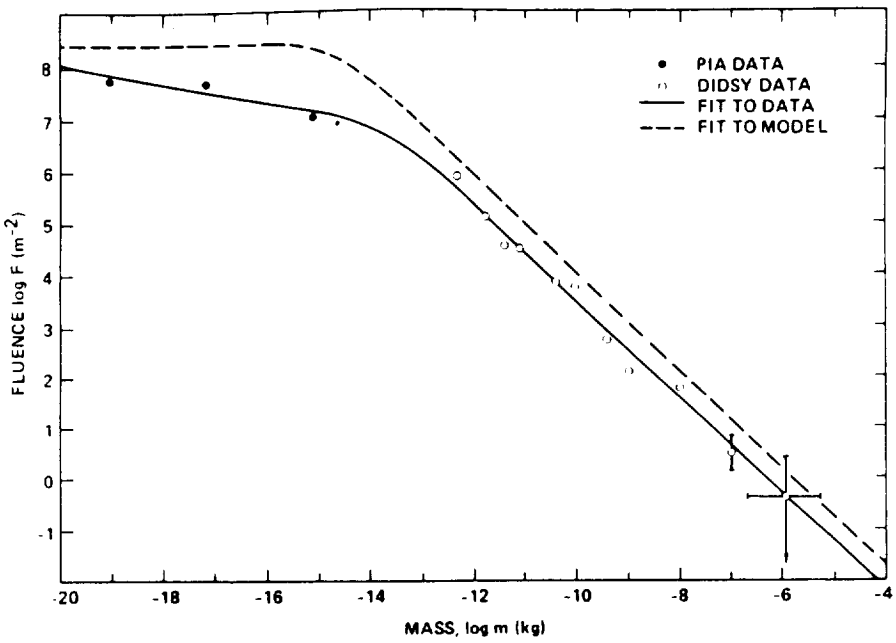

Figure 2.8 - Cumulative fluence versus particle mass from the Giotto DIDSY and PIA experiments, with analytical fit (solid line) from Divine and Newburn (1987). Dashed line is the model with the pre-Halley size distribution (arbitrary fluence or normalization).

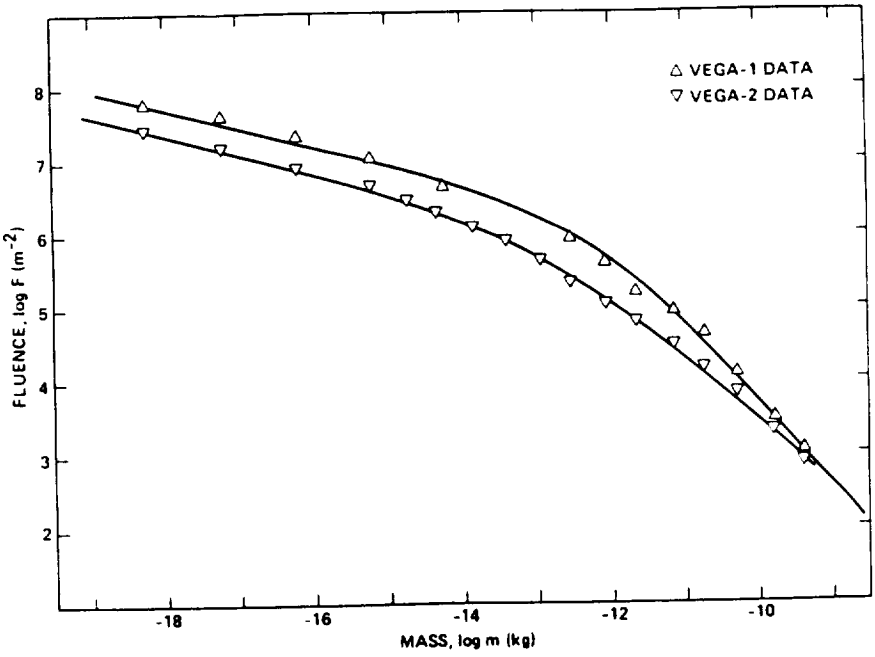

Figure 2.9 - Cumulative mass distribution (fluence) recorded by SP-2 detectors on Vega 1 and Vega 2 with analytical fit by Divine (abstract this report).

encounter and the largest, with their lower velocity, about six hours prior to the encounter. Green proposed that the rate of dust emission decreased, beginning about six hours before Giotto's flyby. Thus, the sensors would sample the higher flux of larger grains from the earlier emission.

The actual size distribution that should be used for modeling the whole coma should not include the excess of large particles measured by DIDSY, since this appears to be a consequence of the velocity dispersion of the grains rather than indicative of the actual mass distribution. According to Green, an extrapolated index of $\alpha \sim 0.9$ would be more representative and would be consistent with the infrared data. However, the Giotto data illustrate that there can be a large dispersion around the average mass-distribution function in the coma.

4.3 Dust Velocity Distribution

To relate the dust density in the coma – whether derived from *in situ* measurements or remote sensing – to the dust production rate from the nucleus requires knowledge of the dust particle velocities, which depend on the gas flux and the mass loading as well as on the particle area/mass ratio. A computed velocity distribution is given by Gombosi (1986) for Halley at 0.8 AU post- perihelion, using a dusty gas dynamic calculation and a mass distribution approximating the *in situ* data. Similar calculations for Halley at several heliocentric distances, based on pre-encounter data, are tabulated by Gombosi *et al.* (1986).

4.4 Dust Particle Density

To convert from the measured mass distribution to the size distribution needed for modeling the optical and infrared remote sensing data, some assumptions about the density of the dust grains are needed. Most likely, the coma contains both compact and fluffy [porous] particles. Table 2-4 summarizes the conversion from power-law-mass distribution to the equivalent size distribution if the density is independent of particle size. The chondritic aggregate IDPs, which seem to be our closest analog to cometary dust, have a filling factor of the order of 0.5, giving a density of ≤ 1 g/cm^3.

Information on the particle density can be derived from the dust-composition experiment on Vega (PUMA) and on Giotto (PIA). The density of pure mineral grains was almost always > 1 g/cm^{-3}, while that of organic grains (CHON particles) was within the limits 0.2 to 1.2 g cm^{-3} (Krueger and Kissel 1987). However, these results refer to small ($\leq 10^{-12}$ g) particles.

Assuming a constant value of 1 g/cm^{-3} for the average density of the particles is probably not wrong by more than a factor of two in either direction over the size range contributing most of the infrared emission, although larger grains may have lower density.

Donn described a fractal aggregate model for the dust; this model leads to a density inversely proportional to particle radius (Donn and Meakin 1987). The fractal model also predicts higher velocities for the larger grains than the models referred to in Section 4.3, because the ratio of mass to cross section for gas drag interaction is smaller than that of spherical grains (Meakin and Donn, abstract this report).

5.0 COMPARISON OF INFRARED DATA WITH MODELS

Various model calculations to fit the observed infrared data were presented at the Workshop. Given the caveats discussed in Sections 1 -4, these models have to be considered preliminary.

5.1 Size Distribution

Although one would like simply to adopt the measured mass distribution to apply to all our observations, it is known from both the *in situ* detectors and the infrared observations that the size distribution varied with time and location in the coma. Moreover, the infrared emission is particularly sensitive to the abundance of roughly micron-sized grains. Yet, this is the region of the inflection in the slope of the mass distribution, whose position is both uncertain and probably variable (SP-1 vs DUCMA on board Vega; Vega 1 vs Vega 2; the gap between DIDSY and PIA on Giotto). If there is more than one dust component, each one may not separately follow the average size distribution (e.g., Clark *et al.* 1986).

In practice, one approach is to adopt Divine's function and vary the parameters as needed to fit the observations, in particular the transition mass, m_t.

5.2 Thermal Emission

Hanner reported on comparisons with the IRTF data taken in March 1986 (Hanner *et al.* 1987). She applied the mass distribution from Giotto, assuming $\rho = 1 g/cm^{-3}$ and omitting the large particle enhancement, to compute via Mie theory the thermal energy distribution (excluding features). Agreement with the data was achieved by shifting m_t by a factor of 2 to 3 toward smaller masses, well within the uncertainties described above.

Mukai (abstract this report) presented models using the Vega 2-size distribution and a "dirty" silicate, whereby the observations of Herter and Tokunaga at 1.3 AU could be matched.

Krishna Swamy reported on two-component models, based on Mie theory, for carbonaceous and coated silicate grains for the full wavelength range from 3 to 160μm (Krishna Swamy *et al.*, abstract this report). He stressed that the low albedo of comet dust and the lack of an obvious 10μm silicate feature in some comets does not necessarily imply a composition dominated by dark carbonaceous material.

Lien (1987 and abstract, this report) has modeled the thermal emission using effective medium theory to compute optical constants for a mixture of silicate and absorbing grains, as described in Section 3.

Glaccum reported on modeling of the long-wavelength infrared data (Glaccum *et al.* 1986). The slope of the spectrum changed from one day to the next, requiring a change in the relative number of small grains. The size distribution fitting the long-wavelength data depends on the assumed emissivity of the grains, which is uncertain due to the problems of clustering discussed in Section 3.

5.3 The 3.4-Micron Emission

At present, it is not known whether the emission feature near 3.36 μm arises from gas molecules or small solid grains. Chyba and Sagan (Chapter 3) proposed that thermal emission from dark organic grains can explain this feature and presented calculations for the thermal emission from small, hot grains having emissivity derived from the transmission spectrum of an irradiated methane ice clathrate residue.

5.4 Polarization

Mukai *et al.* (1987) performed a study of the n,k domain, using Mie theory, to match the observed phase angle and wavelength dependence of polarization. They concluded that n = 1.39 - 1.37 and k = 0.024 - 0.042 at λ 0.37 - 2.2μm provided a good match. (See also Mukai, abstract this report).

Brooke *et al.* (1987 and abstract this report) analyzed the near-infrared polarization, using Mie theory, and concluded that both "dirty" silicate and a more absorbing material were needed.

Lamy *et al.* (1987) concluded that the observed polarization can be reproduced by rough particles, including both dirty silicates and absorbing grains. The negative polarization is introduced by the surface roughness, in contrast to the Mie models, where the negative polarization is caused by silicate spheres (see Section 3.2).

It remains to be shown how valid are the general conclusions about the refractive index deduced from Mie theory for the case of rough, irregular grains.

6.0 COMPARISON WITH INTERSTELLAR DUST IN REFLECTION NEBULAE

As an example of infrared radiation from interstellar grains, Sellgren (abstract this report) summarized the infrared observations of reflection nebulae and the inferences about grain properties from them.

Because the grains are observed at much larger distance from the central star, the equilibrium grain temperatures of $\sim$ 50 K are much colder than the case of comet dust. However, the ultraviolet flux is proportionately higher than in the solar radiation field. Thus, in the near infrared it is possible to observe radiation from non-thermal processes in very small grains or large molecules normally masked by thermal emission.

Strong continuum emission is observed at 1 - 13μm, corresponding to T$\sim$1000 K. Sellgren explains the emission as arising from a component of very small (10 A) particles, temporarily heated by the absorption of a single UV photon (Sellgren 1984). These particles must be refractory enough to survive the occasional ($\sim$ 100 yr) heating from absorbing two UV photons simultaneously.

Reflection nebulae also exhibit the set of six unidentified interstellar emission features, including a strong emission peak at 3.3μm and a broader emission feature extending to 3.4μm. These are thought to arise by ultraviolet pumped fluorescence from polycyclic aromatic hydrocarbon molecules (PAHs) (Leger and Puget 1984; Allamandola *et al.* 1985). These authors propose that overlapping vibrational states in PAH molecules can produce the infrared continuum radiation.

Why the 3.3μm emission is strong in reflection nebulae and other interstellar sources, while it appears as only a weak component compared to the 3.36μm emission in the comet is not yet understood. Further discussion of the 3-micron region in interstellar sources is given by Tokunaga and Brooke, Chapter 3.

REFERENCES

Allamandola, L. J., Tielens, A. G. G. M., and Barker, J. R. (1985). Polycyclic aromatic hydrocarbons and the unidentified infrared emission bands: auto exhaust along the Milky Way! *Astrophys. J.*, **290**, L25.

Bohren, C.F. (1986). Applicability of effective-medium theories to problems of scattering and absorption by nonhomogeneous atmospheric particles. *Jour. Atmos. Sci.* **43**, 468.

Bohren, C.F. & Huffman, D.R. (1983). Absorption and Scattering of Light by Small Particles. Wiley & Sons, New York.

Borghesi, A. Bussoletti, E. and Colangeli, L.(1985). Amorphous carbon grains: laboratory measurements in the 2000A - 40 micron range. *Astron Astrophys* **142**, 225-231.

Brooke, T. Y., Knacke, R. F. and Joyce, R. R. (1987). The near-infrared polarization and color of Comet Halley. *Astron. Astrophys.*, in press.

Chiapetta, P., Perrin, J. M., Torresani, B. (1987). Low energy light scattering: multiple scattering description. *Nuovo Cimento D*, in press.

Clark, B.C., Mason, L.W., Kissel, J. (1986). Systematics of the "CHON" and other light-element particle populations in Comet Halley ESA SP-250, III, 353.

Crifo, J. F. (1987). Optical and hydrodynamic implications of Comet Halley dust size distribution. Brussels Symposium, April 1987, ESA SP-278, in press.

Day, K.L. (1974). A possible identification of the 10 μm "silicate" feature, *Astrophys. J.* **192**, L115.

Day, K.L. (1976) Further measurements of amorphous silicates. *Astrophys. J.* **210**, 614-17.

Day, K.L. (1979). Mid-infrared optical properties of vapor-condensed magnesium silicates. *Astrophys. J.* **234**, 158-161.

Day, K.L. (1981). Infrared extinction of amorphous iron silicates. *Astrophys. J.* **246** 110-112.

Divine, N. and Newburn, R.L. (1987). Modeling Halley before and after the encounters *Astron. Astrophys.* in press.

Donn, B. (1985). Experimental investigations related to the properties and formation of cosmic grains. NASA Conf. Publ. 2403: Interrelationships among Circumstellar, Interstellar, and Interplanetary Dust.

Donn, B. and Meakin, P. (1987). Aerodynamics of fractal grains: implications for the primordial solar nebula. *Bull. AAS* **19**, 847.

Draine, B.T. (1985). Tabulated optical properties of graphite and silicate grains. *Astrophys. J. Suppl.* **57**, 587–594.

Edoh, O. (1983). Optical properties of carbon from the far infrared to the far ultraviolet. Ph.D. dissertation, Dept. of Physics, University of Arizona. (Available through University Microfilms.)

Glaccum, W. Moseley, S. H., Campins, H. and Loewenstein, R. F. (1986). Airborne spectrophotometry of P/Halley from 20 to 65 microns. ESA SP–250, II, 111.

Gombosi, T.I. (1986). A heuristic model of the Comet Halley dust size distribution ESA SP–250 II,167.

Gombosi,T.I., Nagy, A.F. and Cravens, T.E. (1986). Dust and neutral gas modeling of the inner atmospheres of comets. *Rev. Geophys.* **24**, 667.

Hanner, M. S., Tokunaga, A. T., Golisch, W. F., Griep, D. M. and Kaminski, C. D. (1987). Infrared emission from Halley's dust coma during March 1986. *Astron. Astrophys.*, in press.

Huffman, D.R. (1977). Interstellar grains: the interaction of light with a small–particle system. *Adv. in Physics* **26**, 129–230.

Huffman, D.R. (1987). Methods and difficulties in laboratory studies of cosmic dust analogues. Proc. Capri Workshop on Laboratory Studies of Cosmic Dust Analogues, Sept. 1987.

Huffman, D.R. and Stapp, J.L. (1973). Optical measurements on solids of possible interstellar importance. IAU Symp. 52 Interstellar Dust and Related Topics, p. 297–301.

Kerker, M. (1969). The Scattering of Light and Other Electromagnetic Radiation. Academic Press, New York

Khare, B.N. et al (1984). Optical constants of organic tholins produced in a simulated Titanian atmosphere: from soft xray to microwave frequencies. *Icarus* **60**, 127.

Khare, B.N., Sagan, C., Thompson, W. R., Arakawa, E. T., and Votan, P. (1987a). Solid hydrocarbon aerosols produced in simulated Uranian and Neptunian stratospheres. *Jour. Geophys. Res.*, in press.

Khare, B.N., Arakawa, E. T., Thompson, W. R. and Sagan, C. (1987b). Optical constants and spectra of tholins from H_2O - CH_4 gas and H_2O hydrocarbon ices. *Bull. AAS* **19**, 897.

Koike et al (1980). Extinction coefficients of amorphous carbon grains from 2100A to 340 microns. *Astrophys. Space Sci.* **67**, 495–502.

Kratschmer, W. and Huffman, D.R. (1979). Infrared extinction of heavy ion irradiated and amorphous olivine with application to interstellar dust. *Astrophys. Space Sci.* **61**, 195

Krueger, F. R. and Kissel, J. (1987). The chemical composition of the dust of Comet P/Halley as measured by PUMA on board Vega-1. *Naturwissenschaften* **74**, 312.

Lamy, P.L. (1978). Optical properties of silicates in the far ultraviolet. *Icarus* **34**, 68.

Lamy, P.L., Gruen, E., and Perrin, J.M. (1987). Implications of the mass distribution function for the photopolarimetric properties of the dust coma. *Astron. Astrophys.* in press.

Leger, A. and Puget, J. L. (1984). Identification of the unidentified IR emission features of interstellar dust? *Astron. Astrophys.* **137**, L6.

Lien, D.J. (1987). Dust in comets I. Thermal properties of homogeneous and heterogeneous grains. *Astrophys J.* in press.

Mazets, E.P. et al (1986). Dust in Comet Halley from Vega observations. ESA SP-250 II, 3.

McDonnell, J.A.M. et al (1984). The impact of dust grains on fast-flyby spacecraft: momentum multiplication, measurements and theory. *Adv. Space Res.* **4**, No. 9, 297.

McDonnell, J.A.M. et al (1986). Giotto's dust impact detection system DIDSY and particulate impact analyzer PIA: interim assessment of the dust distribution and properties within the coma. ESA SP-250 II, 25.

McDonnell, J.A.M. et al (1987). The dust distribution within the inner coma of comet P/Halley 1982i: encounter by Giotto's impact detectors *Astron. Astrophys.* in press.

Mitra, S.S. & Nudelman, S., eds. (1970). Far Infrared Properties of Solids, Plenum Press, New York.

Mooney, T. and Knacke, R.F. (1985). Optical constants of chlorite and serpentine between 2.5 and 50 microns. *Icarus* **64**, 493–502.

Mukai, T., Mukai, S. and Kikuchi, S. (1987). Complex refractive index of grain material deduced from the visible polarimetry of Comet Halley. *Astron. Astrophys.*, in press.

Perrin, J.M. & Lamy, P.L. (1983). Light scattering by large rough particles. *Optica Acta* **30**, 1223.

Perrin, J.M. & Lamy, P.L. (1986) Light scattering by large particles II. a vectorial description in the eikonal picture. *Optica Acta* **33**, 9.

Perry, C. H. et al. (1972). Infrared and raman spectra of lunar samples from Apollo 11, 12 and 14. *The Moon* **4**, 315.

Philipp, H.R. (1977). Infrared optical properties of graphite. *Phys. Rev.* **B 16**, 2896–2900.

Pollack, J.B. Toon, O.B., Khare, B.N. (1973). Optical properties of some terrestrial rocks and glasses. *Icarus* **19**, 372–389.

Purcell, E.M. and Pennypacker, C.R. (1973). Scattering and absorption of light by non-spherical dielectric grains. *Astrophys. J* **186**, 705.

Sakata, A., Wada, S., Okutsu, Y., Shintani, H., Nakada, Y. (1983). Does a 2,200 Å hump observed in an artificial carbonaceous composite account for UV interstellar extinction? *Nature* **301**, 493.

Sandford, S.A. and Walker, R.M. (1985). Laboratory infrared transmission spectra of individual interplanetary dust particles from 2.5 to 25 microns. *Astrophys. J.* **291**, 838.

Schuerman, D.W., Editor (1980). Light Scattering by Irregularly Shaped Particles. Plenum Press New York.

Schuerman, D.W. (1980). The microwave analog facility at SUNYA: capabilities and current programs. In Light Scattering by Irregularly Shaped Particles. ed. Schuerman, Plenum Press New York, p. 227.

Sellgren, K. (1984). The near-infrared continuum emission of visual reflection nebulae. *Astrophys. J.*, **277**, 623.

Simpson, J.A., Rabinowitz, D, Tuzzolino, A.J., Ksanfomality, L.V. and Sagdeev, R.Z. (1986). Halley's comet coma dust particle mass spectra, flux distributions and jet structures derived from measurements on the Vega-1 and Vega-2 spacecraft. ESA SP-250 II, 11.

Steyer, T.R. (1974). Infrared optical properties of some solids of possible interest in astronomy and atmospheric physics. Ph.D. dissertation, Dept. of Physics, University of Arizona. Available through University Microfilms.

Taft, E.A. and Philipp, H.R. (1965). Optical properties of graphite. *Phys. Rev.* **138** A197–202.

Vaisberg, O., Smirnov, V. and Omelchenko, A. (1986). Spatial distribution of low-mass dust particles ($m < 10^{-10}$ g) in Comet Halley coma. ESA SP-250 II, 17.

Van de Hulst, H.C. (1957). Light Scattering by Small Particles. Dover Publ. New York.

Weiss-Wrana, K. (1983). Optical properties of interplanetary dust: comparison with light scattering by larger meteoritic and terrestrial grains. *Astron. Astrophys.* **126**, 240.

Williams M.W. and Arakawa, E.T. (1972). Optical properties of glassy carbon from 0 to 82 ev. *J. Appl. Phys.* **43**, 3460–63.

Wiscombe, W. and Mugnai, A. (1980). Exact calculations of scattering from moderately nonspherical T_n - particles: comparisons with equivalent spheres. In Light Scattering by Irregularly Shaped Particles, Ed: Schuerman, Plenum Press, New York, p. 141.

Zerull, R., Giese, R.H., Schwill, S., Weiss, K. (1980). Scattering by particles of non-spherical shape. In Light Scattering by Irregularly Shaped Particles, Ed. Schuerman, Plenum Press New York, p. 273.